Chapter 18. Micromagnetic simulations of cylindrical magnetic nanowires

Authors: Yu.P.Ivanov[1] and O.Chubykalo-Fesenko[2,*]

[1] *King Abdullah University of Science and Technology, 23955 Thuwal, Saudi Arabia, ivanov.yup@gmail.com*

[2]*Instituto de Ciencia de Materiales de Madrid, CSIC, 28049 Cantoblanco, Madrid, Spain, oksana@icmm.csic.es*

This chapter reviews micromagnetic simulations of cylindrical magnetic nanowires and their ordered arrays. It starts with the description of the theoretical background of micromagnetism. The chapter discusses main magnetization reversal modes, domain wall types and state diagrams in cylindrical nanowires of different types and sizes. The results on the hysteresis process in individual nanowires and nanowire arrays are also presented. Modeling results are comparing with the experimental ones. The chapter also discusses future trends in nanowires aplications in relation to the simulations, as for example, the current-driven dynamics, spintronics and spincaloritronics. The main micromagnetic programs are presented and discussed together with the corresponding links.

Keywords: magnetic nanowires, micromagnetic simulation, domain wall, reversal mode, magnetic vortex.

1. Introduction

Recent development in nanofabrication has produced a boost in the experimental study of the objects with the scales down from thousands to tens nanometers. It is supposed that

such building blocks of new electronic industry could significantly improve the existing technology.

Magnetic cylindrical nanowires (NWs) constitute an example of such nanotechnology. These NWs with diameters of the order or less than the single domain limit, as well as their arrays, are very attractive for applications in nanoelectronics, energy harvesting, chemical and biological sensing or medicine (Parkin, 2008; Chang, 2007; Liao, 2006; Kim, 2014; Lee, 2012; Schroeder, 2011; Fung, 2008; Song, 2010, Safi, 2011; Choi, 2012; Choi, 2008). NWs with diameters down to 10-20 nm and high aspect ratios can be prepared using electrodeposition into templates, such as nanoporous membranes, which is difficult to achieve by other techniques as, for example, by conventional lithographic processes. Recently another method of growth of the cylindrical NWs using focused beam ion or electron assisted deposition has been developed [Fernandez-Pacheco2013; Serrano-Ramon, 2011; Nikulina, 2012).

Understanding the nature of the magnetization reversal processes in NWs and their arrays is important for the control of their magnetic properties. However, due to very small sizes of NWs, the detailed experimental studies require the use of often expensive equipment or large facilities such as synchrotrons. The experimental measurements on the individual cylindrical (not flat) NWs are non-trivial task. For example, for direct detection of the magnetic configuration, the 3D measurements are necessary. But most of the conventional methods (MOKE, MFM, Lorenz, electron holography, SPEEM) record the 2D data. Micromagnetic simulations are a very powerful tool for the interpretation of such experimental data. Moreover in many cases they can be used prior the experiment, in order to predict experimental results or to check the working hypothesis. Nowadays most of the problems can be solved by a usual modern PC. Moreover, there are several packages available, both open source (Scholz, 2003; Donahue, 2006; Fischbacher, 2007)

and commercial (Scheinfein, 2003; Berkov, 2007), which can be used for running own simulations.

For very small ferromagnetic particles, strictly speaking of the ellipsoidal form (Aharoni, 2000), and with the size less than single domain limit, the Stoner–Wohlfarth model for coherent magnetization rotation has been developed many years ago. Later the disagreement between this model and experiment showed its limitations for high aspect ratio nanoparticles. The coherent reversal has been also investigated as a possible mode for NWs. This mode would correspond to homogeneous rotation of magnetization at unison along the whole length of the NW. Prior to the use of computers, the curling reversal mode was also suggested and evaluated analytically by the pioneer in the micromagnetic theory (Aharoni, 1997) based on the cylindrical symmetry property. His analytical theory for magnetization reversal is valid for homogeneous ferromagnetic prolate spheroid only. He calculated the angular dependence of the nucleation field and coercivity of the high aspect ratio particles for coherent rotation and curling modes for the case of isotropic and anisotropic ferromagnetic material. Later the coherent rotation and the curling reversal modes have become a paradigm in the magnetization reversal studies of nanoobjects and very frequently the experimental results of the angular dependence of coercivity in magnetic NWs are fitted to these models (Fernandez-Pacheco, 2013; Lavin, 2009; Vivas, 2012a; Salem, 2012; Rheem, 2007a; Rheem, 2007b).

More recently the nucleation theory of A.Aharoni has undergone several generalizations in application to NWs. For example, Escrig (2008) have generalized his results, taking into account localized nucleation in the volume of the order of the exchange correlation length. They have discussed three main reversal modes for isolated cylindrical NWs, depending on their geometry: coherent rotation, transverse domain wall (TDW) and vortex domain wall (VDW) modes. The transverse and vortex wall reversal modes

correspond to nucleation and propagation of a domain wall-like (transverse or vortex type) in long NWs. The transition between two last modes is expected to occur with the increase of NWs diameter (Hertel, 2004). These models were successfully fitted to experiments in several cases (Lavin, 2009; Vivas, 2012a). For example, the fitting of the experimentally measured angular dependence of coercivity (Vivas, 2012a; Vivas, 2012b) to models based on TDW or curling within finite volume (similar to VDW) has allowed to associate the coercivity mechanism in Co-based nanowires with possible occurrence of these processes.

However, analytical calculations based on the aforementioned approach can only qualitatively describe the experimental results (Lavin, 2009; Vivas, 2012a; Vivas, 2012b). First of all, the analytical calculations are based on some pre-defined form for the magnetization distribution with trial anzats functions for non-coherent modes. Secondly, the models simplify or do not consider real geometry, structural characteristics of NWs as well as realistic magnetocrystalline anisotropy (MA) and frequently simplify the magnetostatic energy calculation, for example, taking it as an additional shape anisotropy, disregarding the influence of non-homogeneous magnetization distribution.

Micromagnetic simulation is a powerful instrument to investigate the magnetization reversal modes in NWs as well as their ordered arrays (Usov, 1993; Hertel, 2004; Hertel, 2002; Lebecki, 2010, Vila, 2009; Lee, 2007; Forster, 2002; Vivas, 2011; Vivas, 2013; Bran, 2013). These simulations allow the prediction of the reversal mode without any simplifications related to its functional form and magnetostatic fields. The first micromagnetic simulations (Usov, 1993; Belliard, 1998; Hertel, 2004; Hertel, 2002) have corrected the analytical concepts, showing that the reversal in nanowires never takes place by means of coherent rotation or curling but by the nucleation of domain walls at the ends of NW and subsequent depinning and propagation along its length. The DW structure is

TDW or VDW depending on the NW diameter (Hertel, 2004). The TDW occurs in NWs with small diameter while for larger diameter the reversal takes place by means of the VDW. In larger micron-size NWs the reversal modes can have even more complex structure (Usov, 1998; Stoleriu, 2012).

Experimentally TDW and VDW were previously observed in magnetic nanostripes (the nanowires with rectangular cross section and relatively small thickness in comparison with the width and length of the NW) (Boulle, 2011). The spin configuration of such NWs can be described in 2D. Strictly speaking, the TDW and VDW spin configurations in nanowires with rectangular and cylindrical cross-section are different and should be distinguished. However, historically, the same names are used. Recently domain walls in cylindrical nanowires have been observed by means of X-ray circular magnetic dichroism (Da Col, 2014). The understanding of the magnetic structure in these objects is more complicated due to a 3D nature of spin configuration. To distinguish VDW in 3D from the VDW in nanosripes, Da Col (2014) proposed to call VDW in cylindrical NWs as a Bloch-point DW. The DW propagation in cylindrical NWs according to (Thiaville 2003; Hertel, 2004) can be described as a Bloch-point nucleation and propagation. The Bloch-point is a singularity sitting on the core of the VDW where the magnetization is changed from the up to the down direction, strictly speaking passing through zero magnetization. The magnetization reversal through the Bloch point makes the magnetic configuration in such NWs very stable versus thermal fluctuations since the corresponding energy barrier separating the two states is very high. In addition, recently it has been shown that in NWs with strong uniaxial magnetocrystalline anisotropy the remanent magnetization can be characterized by the vortex-like configuration in the whole NW, depending on the direction of the magnetocrystalline easy axis in respect to the NW axis (Ivanov, 2013a).

This chapter is organized as follows. In section 2 the theoretical background of micromagnetism is presented and some technical aspects related to the finite differences and finite element methods are briefly discussed. Section 3 is devoted to description of the main reversal modes, domain wall types and state diagrams in cylindrical nanowires. In section 5 we will describe some results on the hysteresis process in individual nanowires and nanowire arrays. Modeling results will be compared with the experimental ones. The role of magnetostatic interactions will be also discussed. Section 5 is devoted to describing future trends in nanowires in relation to the simulations, as for example, the current-driven dynamics, spintronic and spincaloritronic applications. Future possibilities for modeling of microwires using large computer resources and graphical cards will be outlined. Main micromagnetic programs and their web pages are highlighted in section 6.

2. Micromagnetic model

Micromagnetism is a continuum theory of ferromagnetic materials that allows for the computation of spin configuration of the samples with arbitrary shape. The theory is based on the assumptions that the length of the magnetization vector is constant and all energies vary slowly at the atomic scale. Thus this theory is very suitable for nano objects but breaks down approaching the atomic size. The assumption of the constant magnetization length also restricts the theory for temperatures far from the Curie temperature.

The micromagnetism is based on the energy minimization. Most of micromagnetic programs either uses a direct energy minimization by means, for example, of conjugate-gradient method or solves the dynamical equation of motion. The dynamics of the magnetization vector in external magnetic field is described by the Gilbert equation (Brown,1963a)

$$\frac{dm}{dt} = -\gamma_0\left(m \times H_{eff}\right) + \alpha[m \times \frac{dm}{dt}]$$

where m is the (normalized) magnetization vector, γ_0 is the (positive) gyromagnetic ratio, α is the Gilbert damping parameter and H_{eff} is defined as the effective field. It consists of the external magnetic field and the contributions of the exchange, magnetic anisotropy and magnetostatic energies. H_{eff} can be represented as the first derivative of the total energy density in respect to the magnetization

$$H_{eff} = -\frac{1}{\mu_0 M_s}\frac{\partial E}{\partial m}$$

where Ms is the saturation magnetization. The total energy of the ferromagnetic element (particle) includes exchange, magnetic anisotropy, magnetostatic and Zeeman energies contributions and can be written in the international system of units as follows

$$E = \int_v E(m)dV = \int_v A(\vec{\nabla}\,\vec{m})^2 dV + \int_v E_a dV$$

$$- \frac{1}{2\mu_0 M_s}\int_v \left[\vec{m}\cdot\vec{H}_{dem}(\vec{m})\right]dV - \mu_0 M_s \int_v \left[\vec{m}\cdot\vec{H}_{app}\right]dV$$

Here A is the exchange constant, μ_0 is the vacuum permeability, E_a is the anisotropy energy, H_{dem} is the magnetostatic field and H_{app} is the external magnetic field. Depending on the anisotropy type the second term can be written as

$$E_{a,u} = -K_u(\overrightarrow{u_k}\vec{m})^2$$

for uniaxial anisotropy, where K_u is the uniaxial anisotropy constant and u_k is the unit vector along the anisotropy axis, or

$$E_{a,c} = K_1(\alpha^2\beta^2 + \beta^2\gamma^2 + \alpha^2\gamma^2) + K_2(\alpha^2\beta^2\gamma^2)$$

for cubic anisotropy, where K_1 and K_2 are the cubic anisotropy constants and α, β and γ are the directional cosines of the magnetization in respect to the cubic easy axes.

For numerical integration the Gilbert equation (1) is converted into the Landau-Lifshitz-Gilbert (LLG) equation and used in the following form

$$(1+\alpha^2)\frac{dm}{dt} = -\gamma_0[(m \times H_{eff}) + \alpha m \times (m \times H_{eff})].$$

The first term on the right-hand-side corresponds to the gyroscopic behavior and the angular momentum associated with the interaction between the magnetization and H_{eff}. Dissipation of the energy is given by the second term often in a phenomenological sense. In the case of hysteresis simulation this term is introduced to make the system to go down to the equilibrium state.

In order to find the equilibrium state or to solve for the dynamics, a sample with specific finite shape is divided into cubic cells (finite-difference, FD simulations) or finite elements, FE. The magnetization is specified either as the value in the center of the cube (representing the average value over this portion of the volume) or as the value on the nodes. In the latter case the magnetization is continuously interpolated inside the element. The initial state of all these cells is defined before starting the simulation. The evolution of the system is calculated either by direct energy minimization or by integrating the LLG equation in time for each cell. The calculation is finished until the Brown condition (Brown, 1963b) is reached.

One of the main criteria which have to be rigorously taken into account is the size of the cubic cells or average size of the finite elements. For small anisotropy materials, they must be smaller than the exchange correlation length l_{ex} of the simulated material. The l_{ex} is defined as :

$$l_{ex} = \sqrt{\frac{2A}{\mu_0 M_s^2}}$$

Exchange lengths for typical materials of the cylindrical NWs and other relevant parameters are presented in table 1.

Table 1. Parameters of typical materials of the cylindrical NWs. The anisotropy direction for cubic anisotropy is characterized by the Euler angles (θ; φ; ψ) (rad), where: θ and φ are angles which form the magnetocrystalline anisotropy axes in spherical coordinates with x and y axes, the z axis coincides with the NW axis and ψ is the third Euler angle.

Material	**Crystal structure**	**A (J/m)**	**M_s (T)**	**L_{ex} (nm)**	**Anisotropy type**	**Easy axis (θ; φ; ψ) (rad)**	**K_a (J/m^3)**
Py($Fe_{80}Ni_{20}$)(Smith, 1989)	polycrystalline	1.05e-11	1.0	5.1	-	-	0.0
Ni(111) (Liu, 2005)	fcc, [111] // NW axis	0.34e-11	0.61	4.8	cubic	[111], (0.96;0; 0.61)	-0.048e5
Fe(110) (Liu, 2005)	bcc, [110] // NW axis	0.81e-11	2.15	2.1	cubic	[110], (0;0; 0)	0.48e5
Fe(100) (Liu, 2005)	bcc, [100] // NW axis	0.81e-11	2.15	2.1	cubic	[110], (0.79;0;0)	0.48e5
Co(111) (Fisher, 1970)	fcc, [111] // NW axis	1.30e-11	1.75	3.3	cubic	[111],(0.96;0; 0.61)	-2.7e5 -0.75e5
Co(100) (Cullity, 1972)	hcp, polycrystalline, texture (100)	1.30e-11	1.75	3.3	easy plane, ⊥NW axis	random 2D in-plane	4.5e5
Co-hcp (Cullity, 1972)	hcp, polycrystalline	1.30e-11	1.75	3.3	easy axis in each grain	random 3D	4.5e5
Fe80Co30 (Bran, 2013a)	bcc, polycrystalline	1.08e-11	2.0	2.6	easy axis in each grain	random 3D	0.1e5
Fe86Ga14(100) (Reddy, 2011)	bcc, [110] // NW axis	2.06e-11	1.6	4.5	cubic	[110],(0.0;0.0; 0.0)	0.3e5

The most time-consuming part of micromagnetic simulations is the calculation of the magnetostatic field. A lot of efforts has been devoted to develop the efficient methods for calculating the magnetostatic contribution. Nowadays there are several approaches. The most frequently used ones are the FEM-BEM (finite-element-boundary element) method,

used for FE and the fast Fourier transform or the fast multipole expansion method used for FD. The important practical difference between the finite elements and finite difference methods is the possibility to treat curved geometries which are better suited for the finite elements. Fig. 1 shows the examples of the FE and FD meshing of the cylindrical NW. Clearly, the FE discretization is more suitable for modeling of NWs with cylindrical geometry.

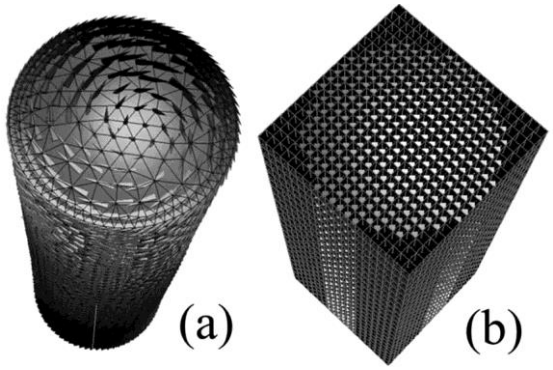

Figure 1. The examples of NW meshing in the case of FE simulation (a) or FD simulation (b).

Additionally, for meaningful micromagnetic model, the appropriate crystal structure in terms of the type of the magneto-crystalline anisotropy, its constant value and easy axis directions and distribution must be taking into account. In the table 1 the parameters of typical materials of cylindrical NWs are presented. Note that the so-called shape magnetic anisotropy is a part of the magnetostatic energy and thus should not be included explicitly into the anisotropy term. This makes it difficult the extraction of the anisotropy parameter from the hysteresis cycle measurements since the so-called “effective anisotropy” is the sum of all possible contributions, including the magneto-crystalline and the “shape” one. The quantitative agreement between simulation data and experimental ones strongly

depends on the inclusion of realistic experimental nanostructure and parameters into the model (Vivas, 2013; Ivanov, 2013a).

Micromagnetic simulation are very demanding in terms of computer resources. The first resource is the amount of the RAM available in the computer system. Since the cell size must be around few nanometers, a large structure can significantly increase the number of cells and consequently the RAM needed. The NWs with 40 nm diameter and 2 μm length may consume up to 1 Gb of RAM. The model used in FE packages pre-calculate the magnetostatic energy matrix and requires even higher RAM. In order to keep the time required to simulate a large structure at a minimum, the processor must be able to fully access the data in RAM as fast as possible. Thus, in order to minimize the time taken by a simulation, the use of the parallel computing is desirable. The major micromagnetic programs have in nowadays parallel versions.

3. Reversal modes in cylindrical nanowires

First, let us discuss the reversal modes of the NWs with negligible or very small magnetocrystalline anisotropy. These will correspond to NWs with polycrystalline structure or single crystal NWs with cubic anisotropy such as permalloy or Ni NWs. Fig. 2 shows the reversal modes diagram (Ivanov, 2013b) presented in terms of the NW diameter and the material type /defined by the exchange correlation length) calculated by the MAGPAR finite element micromagnetic package. The NWs have been represented as cylinders of 2 μm fixed length and diameters were varied from 20 to 100 nm thus saving a high aspect ratio of NWs and which therefore exhibit strong shape anisotropy. They are discretized in a tetrahedral mesh, and the magnetization orientation is computed on each mesh vertex. The structure, anisotropy and magnetic parameters of NWs are shown in table 1. For the simulation of polycrystalline NWs a random orientation of magnetocristalline easy axis in each tetrahedral has been considered. The average finite element discretization size was chosen 4 nm.

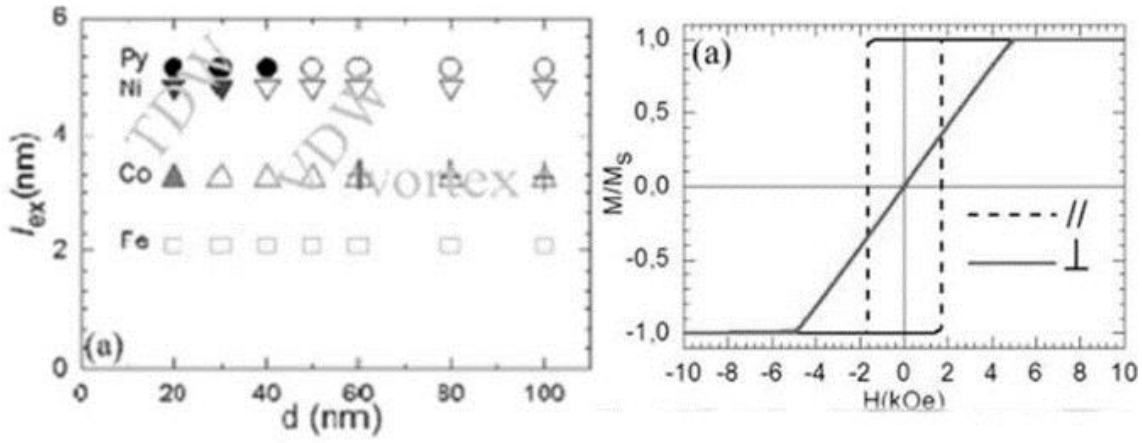

Figure 2. (a) The diagram of the DW type in polycrystalline (Co, Py) and single crystalline cubic anisotropy (Co, Fe,Ni) NWs.The fill points and open points are TDW and VDW, accordingly. The cross rectangles indicate the area with magnetic vortex state spanning the whole NW length at the remanence and quasi-curling reversal mode for hcp

Co NWs polycrystalline The field is applied parallel to NW axis. (b) The typical hysteresis loops simulated for NWs which magnetic behavior is mostly determined by the shape anisotropy.

The magnetization reversal of NWs with polycrystalline structure or with single crystalline cubic anisotropy is mostly determined by the shape anisotropy due to its high value with respect to the averaged magnetocrystalline one. This high value is caused by the high aspect ratio length/diameter. Typical hysteresis loops for magnetic field applied parallel ∥ and perpendicular ⊥ to the NW axis are presented on fig.3. For the ∥ case, the loop has a rectangular shape and the magnetisation reversal occurs by the DW propagation. The type of the DW changes from TDW to VDW depending on the l_{ex} and NW's diameter. For example, for Fe NWs only VDW is observed, while for Co NWs the transition occurs at 20 nm diameter and for Py NWs at 40 nm. Recently the transition of the TDW to VDW in cylindrical NWs has been experimentally observed by electron holography (Biziere, 2013) and XMCD-PEEM (Da Col, 2014) in a good agreement with diagram presented on fig.2. The remanence is the single domain state with the magnetization aligned along the NW axis. Only at the NW's ends the spins form vortex-like configuration – the so-called open vortex structure. The length of this area at the ends is also dependent on the material. It is larger for the materials with smaller l_{ex} and increases with the NW diameter. Particularly, one should remember that the formation of such structures at the NW's ends, minimizing the magnetostatic energy, does not allow the estimation of the shape anisotropy using simple analytical expressions. Fig. 3 shows the structure of the DWs and open vortex structure at the remanence.

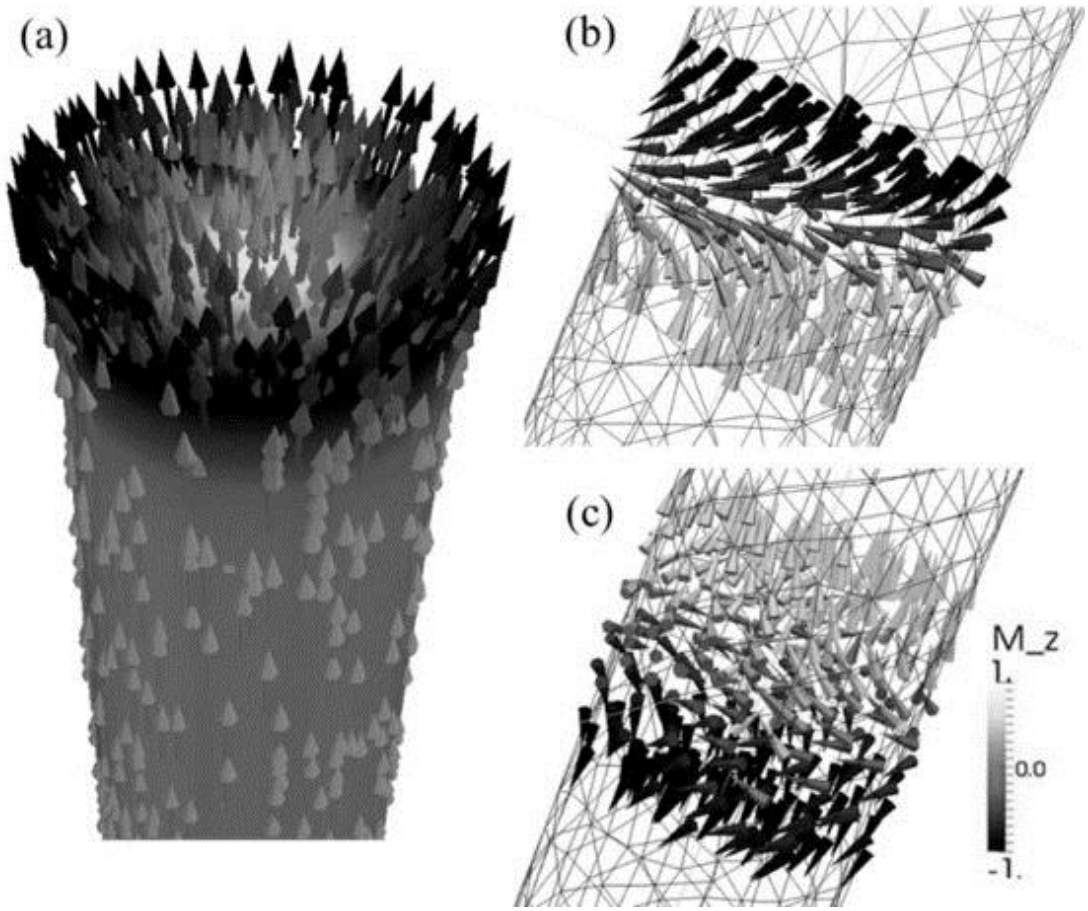

Figure 3. (a) The open vortex structure at the NW's end at remanence. (b) – (c) TDW and VDW of the cylindrycal NW.

Figure 4 shows the coercivity, Hc, and the reduced remanence, Mr/Ms, as a function of the NW diameter in the case of magnetic field applied parallel (//) to the NW axis, simulated for series of NWs with different crystalline structure. Mr/Ms is slightly reduced with the NW diameter and this effect is a bit more pronounced for material with smaller l_{ex}. It is connected with the aforementioned above appearance of the open vortex area at the NW's ends.

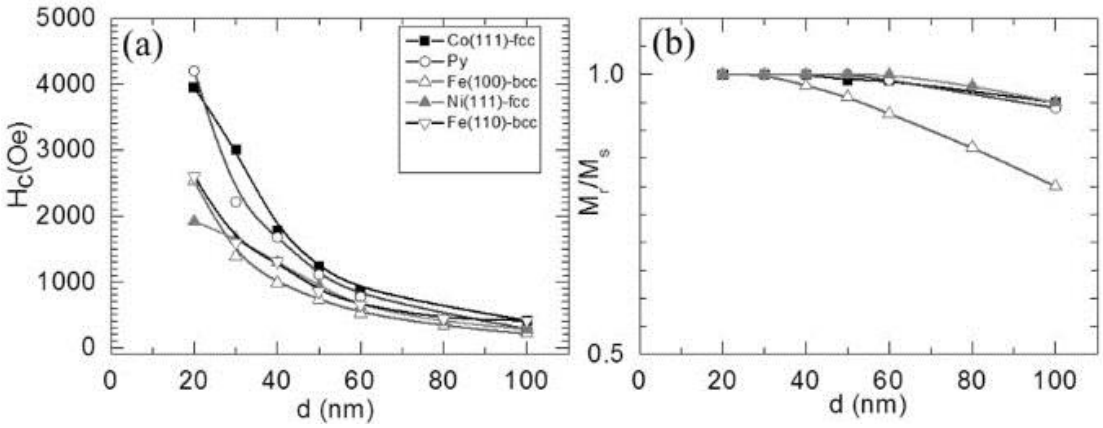

Figure 4. The magnetic parameters (coercivity Hc and the remanence Mr/Ms) as a function of the NW diameter for magnetic field applied parallel to the NW axis for series of polycrystalline and single crystalline NWs with cubic anisotropy.

As shown on fig.4a for all NWs the coercivity decreases with the increase of the NW diameter as corresponds to the decrease of the shape anisotropy which scales with the ratio length/diameter. Note that for the smallest diameters the coercivity of Co and Py NWs is twice larger than for Ni and Fe NWs, which is related to the change of the magnetic reversal mode as shown on the diagram, fig. 2(a). In general the coercivity value for the TDW mode is higher than for VDW mode. Similar effect can be observed for the same material and fixed NW's diameter under, for example, annealing. In (Bran, 2013b) it has been reported that the coercivity of the CoFeCu NWs was increased after annealing at 500 ^{0}C which can be attributed to the decrease of the Ms value and consequently the increase of l_{ex}.and the transition of the reversal mode from VDW to TDW.

The data represented in fig. 4 are in a good agreement with those reported in the literature from experimental data for NWs with the same geometry and crystal structure (see table 2). Small discrepancies between experimental results and our micromagmetic simulations can be attributed to the change of MA due to the different crystal quality of NWs prepared

at different electrodeposition conditions. Also, as shown in figure 4, for Fe NWs with different easy axis orientations and for Co NW the coercivity value cannot change too much with the crystal quality of NWs, especially for NWs diameters larger than 50 nm. Our simulations show that the change of cubic anisotropy in three times, as presented in table 1, does not affect too much the magnetic properties of fcc Co nanowires. The data presented in figure 4 can be also applied to the NWs based on Fe, Co, Ni alloys, taking into account that correct simulation parameters can be varied depending on the alloy composition (Bran, 2013a) and would change slightly the resulting coercivity value.

Table 2. Comparison between simulated coercivity values in various NWs with reported in the literature.

Material	**d (nm)**	**Aspect ratio**	**Length (nm)**	**H_c (Oe)**	
				simulation	**experiment**
Py($Fe_{80}Ni_{20}$)	35	60	2000	1900	1232 (Navas, 2005)
	40-70	80	5000	1620-670	1436-700 (Salem, 2012)
Ni(111)	20	50	1000	1900	970 (Zheng, 2000)
	35	60	2000	1350	780 (Navas, 2005)
	30	30	700	1550	1200 (Nielsch, 2002)
	50	240	12000	927	624 (Escrig, 2008)
	30-100	20	2000	1550-290	1150-300 (Fert, 1999)
	30,40,55	20	1000	1620,1255,740	1200,1000,600 (Nielsch, 2001)
	180	20	3400	290	215 (Escrig, 2007)
	50	1000	50000	927	1000 (Pan, 2005)
Fe(110)	70	20	1000	555	550 (Haehnel, 2010)
	20	50	1000	2500	2250 (Sellmyer, 2001)
	80	70	5000	455	450 (Wang, 2004)
	30	170	5000	1700	1720 (Wang, 2004)
Fe(100)	35	120	4000	1245	1250 (Yang, 2000)
	20	200	4000	2321	2311 (Paulus, 2001)
Co(111)	40	10	120	1790	1730 (Vazquez, 2011)
	40	130	5000	1790	1760 (Zhang, 2007)

In the case of magnetic field applied perpendicular ⊥ to the NW axis the magnetic behavior of NWs is practically non-hysteretic (figure 2b) and magnetic parameters are

almost independent on the NW diameter. The reversal mode is the quasi-coherent rotation. The spins on the open vortex area are not following the direction of the applied magnetic field simultaneously with those in the inner structure.

Magnetocrystalline anisotropy (MA) can be used as a very efficient instrument to control the magnetic behavior of the cylindrical nanowires (Vivas, 2013; Ivanov, 2013a; Henry, 2001; Lui, 2008). For the efficient control of magnetic properties via engineering of the magnetocristalline anisotropy, its constant should be large enough to compete with the shape anisotropy of the high aspect ratio NWs. Since the strength of the magnetocrystalline anisotropy is strongly affected by crystal quality of the NW's, the best samples to compare with theory are the single crystalline NWs. For example, Co NWs frequently show a preferential, almost single crystal, hcp crystallographic structure (Pan, 2005; Henry, 2001; Lui, 2008). The presence of such crystal phase leads to a noticeable uniaxial MA of the same order of magnitude ($4.8x10^5$ erg/cm^3) as the shape anisotropy. Depending on the orientation of MA easy axis in respect to the NW axis, the MA can both increase and decrease the effective anisotropy of NWs. Consequently, the magnetic properties of Co NWs can be tuned by modifying the crystal growth direction (Vivas, 2012b; Vazquez, 2011; Henry, 200)1 or NWs composition (Co-based alloy NWs) (Vivas, 2012a; Bran, 2013a; Vega, 2012).

Figure 5(a) shows the diagram of DW type as a function of the NW diameter for Co hcp single crystalline NWs in //-field configuration. Single crystal NWs with the orientation of MA easy axis (c-axis) at different angles θ in respect to the NW axis have been considered. Strong uniaxial MA in single crystalline hcp-based NWs significantly affects the magnetic reversal mode.

The TDW reversal mode is stabilized by MA with easy axis at $0^0 \leq \theta \leq 60^0$ in the whole range of NW diameters. In $\perp$-field configuration the quasi-coherent rotation mode is observed in that case.

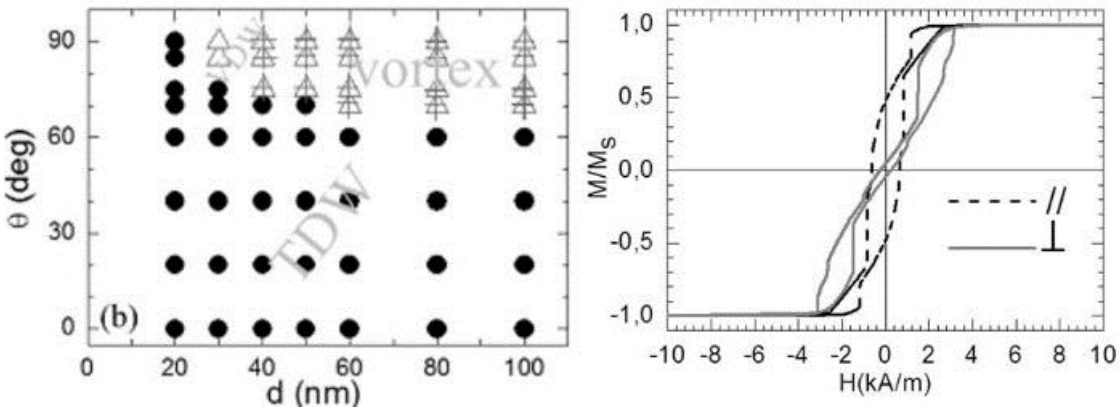

Figure 5. (left) The diagram of the DW type in single crystall hcp Co NWs with easy axis direction at the angle θ with the NW axis as a function of the NW diameter is shown. The filled circles and open triangles stand for TDW and VDW, accordingly. The crossed triangles indicate the area with magnetic vortex state spanning the whole NW length at the remanence and the quasi-curling reversal mode. The field is applied parallel to the NW axis. (right) The typical magnetic loops simulated for NWs with competing shape and magnetocrystalline anisotropies. The simulations correspond to an individual single crystal hcp Co NW with θ=880.

For $70^0 < \theta < 90^0$ there is a transition between the two wall types and the transition diameter decreases significantly with θ. Note that for the narrowest NWs (20 nm diameter) the reversal mode is TDW propagation independently on the MA easy axis orientation.

Another transition for the reversal mode can be induced by the MA with easy axis at $0^0 \leq \theta \leq 60^0$ for Co NWs with large diameters. Here a quasi-curling reversal mode appears [shown as crossed triangles in figure 5(a)]. In that case the spins at the remanence form a

vortex-like state along the whole NW length (see figure 6) with a core parallel to the initial applied field direction in // configuration or randomly oriented up/down in ⊥ configuration. Due to the high aspect ratio of NWs there are several vortices with alternating chiralities (clockwise/ counterclockwise) along NW length (see figure 6). Note that for the ⊥ configuration the number of vortices is larger than for // configuration. The same transition is also observed for textured Co(100) hcp NWs with the easy plane anisotropy in-plane of NW diameter (Ivanov, 2013b). The corresponding mode is called quasi-curling because of different speed of the curling at the NW ends and in the center. The core of the vortex is remagnetized by domain wall nucleation and propagation.

Figure 6. (a) The vortex structure at the remanence of the single crystall hcp Co NW with c-axis oriented at 880 in respect to NW axis.

Typical hysteresis loops simulated for NWs with competing shape and magnetocrystalline anisotropies are presented in figure 5b. As shown in figure 7, the magnetic behavior of Co hcp NWs strongly depends on θ in the interval between 75 and 90 degrees. For $\theta<70^0$ the MA reinforces the shape anisotropy. When the field is applied parallel to the NW axis, the coercivity is increased as compared with polycrystal NWs and decreases practically linearly with the NW diameter [figure 7a], following the behavior of the shape anisotropy. At $\theta > 70^0$ the MA tends to compensate the shape anisotropy and both the coercivity and the remanence decrease drastically with the NW

diameter. The strong decrease of the remanence is associated with the formation of the vortex state along the whole NW length (see figure 6). Note that recently the existence of the vortex state along the whole NW has been confirmed by the MFM measurements (Ivanov, 2013a). The tilt of the anisotropy in respect to the NW axis makes the vortex structure loose its circular symmetry and produces visible by MFM magnetic charges.

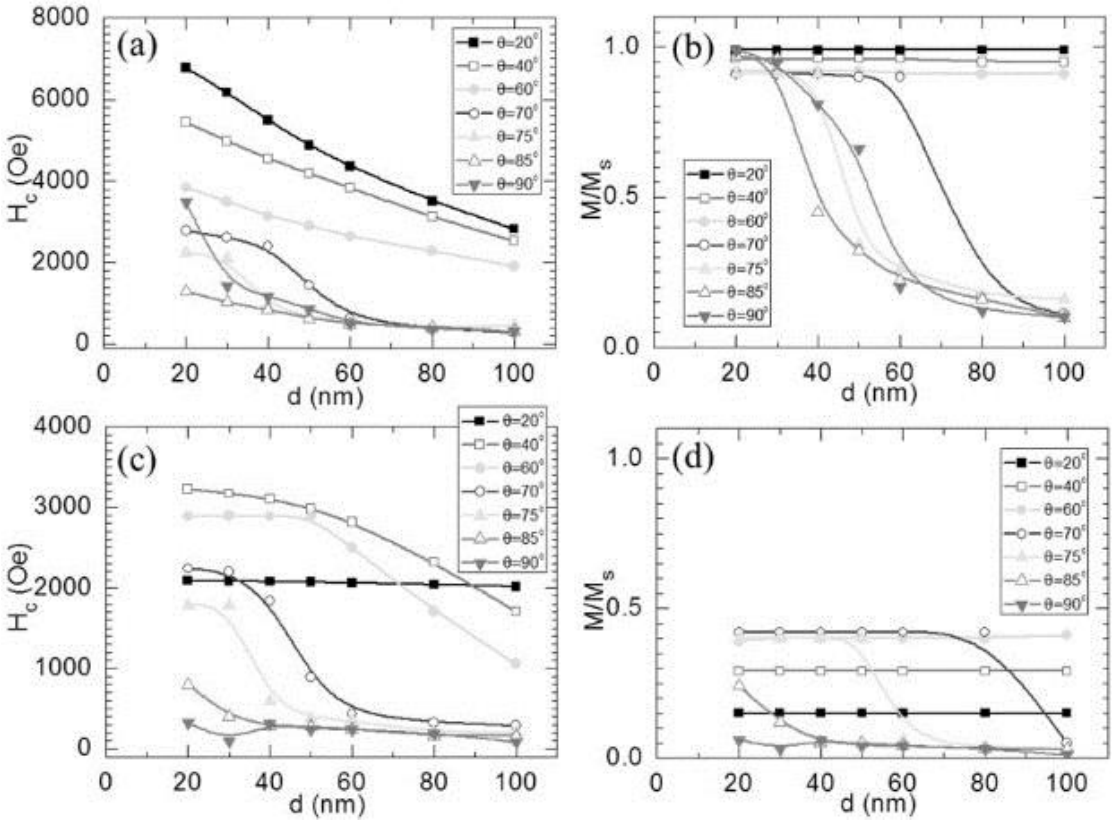

Figure 7. The magnetic parameters (coercivity Hc and the remanence Mr/Ms) as a function of the NW diameter in the case of magnetic field applied parallel (a)-(b) and perpendicular (c)-(d) to the NW axis for single crystal Co hcp NWs and different easy axis orientations (defined by the angle θ with NW axis).

It is common to use the angular dependence of coercivity to elucidate the occurrence of different magnetic reversal modes in NWs (Fernandez-Pacheco, 2013; Lavin, 2009;

Vivas, 2012a; Salem, 2012; Rheem, 2007a; Rheem, 2007b). For this purpose, the magnetic loops are measured at the different directions of the applied magnetic field in respect to the NW axis (defined by the angle α) for hexagonal ordered arrays of NWs (Lavin, 2009; Vivas, 2012a; Salem, 2012) or single NW (Fernandez-Pacheco, 2013; Rheem, 2007a; Rheem, 2007b). After that the data can be fitted using the analytical expressions for nucleation field (Lavin, 2009; Vivas, 2012a; Salem, 2012; Rheem, 2007a; Rheem, 2007b). Specifically, Vivas (2013a) basing on analytical models, have concluded about the transition between TDW and VDW modes in CoNi-alloy NWs as a function of the applied field angle.

Another approach is to use the micromagnetic simulation with the realistic model parameters (geometry, material properties, magnetocrystalline anisotropy). In Ivanov (2013b) the simulations of the angular dependence of the critical fields (nucleation field Hn and coercivity Hc) and the remanence Mr/Ms for NWs with different reversal modes, based on Py, Fe(110) and Co (easy axis angle $\theta=88^0$) with 40 nm diameter, as well as for hexagonal ordered array of 7 NWs with the center-to-center distance between NWs being 105 nm have been performed. According to the diagram in figure 2(a), the reversal mode corresponds to the TDW propagation for Py and VDW propagation for Fe(110) and quasi-curling mode for Co NWs, when the field is applied parallel to the NW axis. In simulations with field applied at different angles, the change of the reversal mode type with the applied field angles was not observed, except for the exact value $\alpha=90^0$, when the TDW or VDW mode is changed to quasi-coherent rotation mode.

Importantly, the simulations showed the differences between the angular dependence of the nucleation and the coercivity fields Hn and Hc. For large applied field angles, Hc is not equal to Hn in agreement with the experimental data reported by numerous authors (Escrig, 2008; Yang, 2000; Paulus, 2001). Their angular dependence is the same in the

range of the applied field angles $0^0 \leq \alpha \leq 60^0$. However, for $60^0 \leq \alpha < 90^0$ the two fields are different: the Hn starts to increase, while the Hc decreases. The angular dependence of Hc is similar to the curling reversal mode although, but in fact, the VDW or TDW occur for all angles. Based on analytical formula, the functional dependence of coercivity in CoNi nanowires, has been interpreted as a change of the reversal mode from TDW to VDW at 60 deg (Vivas, 2012a) while the micromagnetic simulations report the same trend but do not show such a transition .

Finally, we summarize the type of the DWs in cylindrical NWs extracted from micromagnetic simulation (Ivanov, 2013b). For NWs with a weak magnetocrystalline anisotropy (polycrystalline NWs or single crystal NWs with a cubic anisotropy) two types of the DW are dominated: TDW and VDW (called also the Bloch-point DW). Both of them can be also in head to head or tail to tail configuration. NWs with 3D vortex structure along the whole NW length (single crystal hcp Co NWs) present two different DWs at the interface between two vortices with opposite chiralities of the vortex shell or polarities of the vortex core: chirality to chirality or polarity to polarity. The orientation of the spins in the region between two vortices (DW) with opposite chirality or polarity depends on the type of magnitocrystalline anisotropy. For single crystal hcp Co NWs the spins in the center of the DW are aligned parallel to the easy axis direction (c-axis) while for polycrystaline hcp Co NWs, governed by the shape anisotropy, the spins in the center of DW are directed parallel to the NW axis. These types of the DW is called also in literature helical DWs (Sekhar, 2012).

4. Simulation of hysteresis in individual nanowires and nanowires arrays.

The most promising application of the cylindrical NWs include the NWs assembling in ordered arrays. Therefore the question about dipole-dipole interaction between NWs becomes very important. Most of the reported arrays are the hexagonal with the typical parameters diameter/interpore distance: 20-40nm/55nm, 35-80 nm/105 nm, 120-200nm/200 nm.

Frequently the strength of the dipole-dipole interaction in ensembles of nanomagnets is estimated by measuring the first-order reversal curves (FORC) diagrams (Mayergoyz, 1985; Stancu, 2003; Spinu, 2004). In particular the FORC analysis used in the Vivas (2012a) indicated the presence of intense dipolar magnetic fields for Co NWs when compared to the CoNi ones. The authors attributed this effect to the increase of the axial anisotropy due to the addition of Ni.

Theoretical calculation of the magnetostatic field in NW's arrays is very complicated due to the inhomogeneous spin structure of the NW and its change in applied magnetic field. In the case of the homogeneously magnetized NWs whose magnetic behavior is determined by the shape anisotropy, the magnetostatic interaction up to 70000 NWs has been calculated numerically assuming each NW as one macrospin pointed up or down (Escrig, 2008). In real array the situation is more complicated, mostly due to the specific magnetic structure of each NW in the array. Clearly the magnetic state of the nanowire should influence the strength of magnetostatic interactions. Indeed, the vortex state presents practically no surface charges and thus the magnetostatic interactions between NWs are substantially reduced. Similarly, the presence of open vortex structure as those presented in Fig.3a at the end of NW which is mostly magnetized along its length, should considerable reduce the magnetic flux, as compared to idealized homogeneously

magnetized NWs as those discussed above. This also invalidates the use of the demagnetization factor approach to include magnetic interactions into consideration.

Micromagnetic simulation is potentially ideal instrument to estimate the magnetostatic interaction inside the NW's array. But the number of NWs which can be taken into account is very limited by the computational power. Thus, most of simulations have been performed in individual NWs or an array of 7 NWs The calculations of arrays of up to 49 NWs is reasonably possible using parallel computers. However, the influence of interactions can be already seen in the modeling of 7 NWs. Our experience shows that the parallel loops are only slightly modified by the presence of interactions, for example, in terms of the saturating field value. However, the perpendicular, i.e. in-plane, hysteresis loops are very sensitive to interactions, due to the influence of the thin film geometry producing an additional "thin film" anisotropy.

Figure 8 shows the hysteresis loop simulated for an individual NW and hexagonal ordered array of 7 NWs. The nanowire diameter (D) is 40 nm and intertwire distance is 105 nm. In general if the distance between NWs is larger, the magnetostatic interaction is practically negligible. The coercivity and the remanence of single NW and NW's array are only slightly different. More inclined magnetic loops are calculated in the array as compared to individual NWs for NWs with strong competition of magnetocrystalline and shape anisotropy (fig. 8 c,d) which indicates a stronger interaction between NWs in contrast to the case of NW which magnetic behavior is determined only by the shape anisotropy (fig. 8c,d). The calculated angular dependence of the coercivity and the remanence for single NW and NW's array are also quite similar.

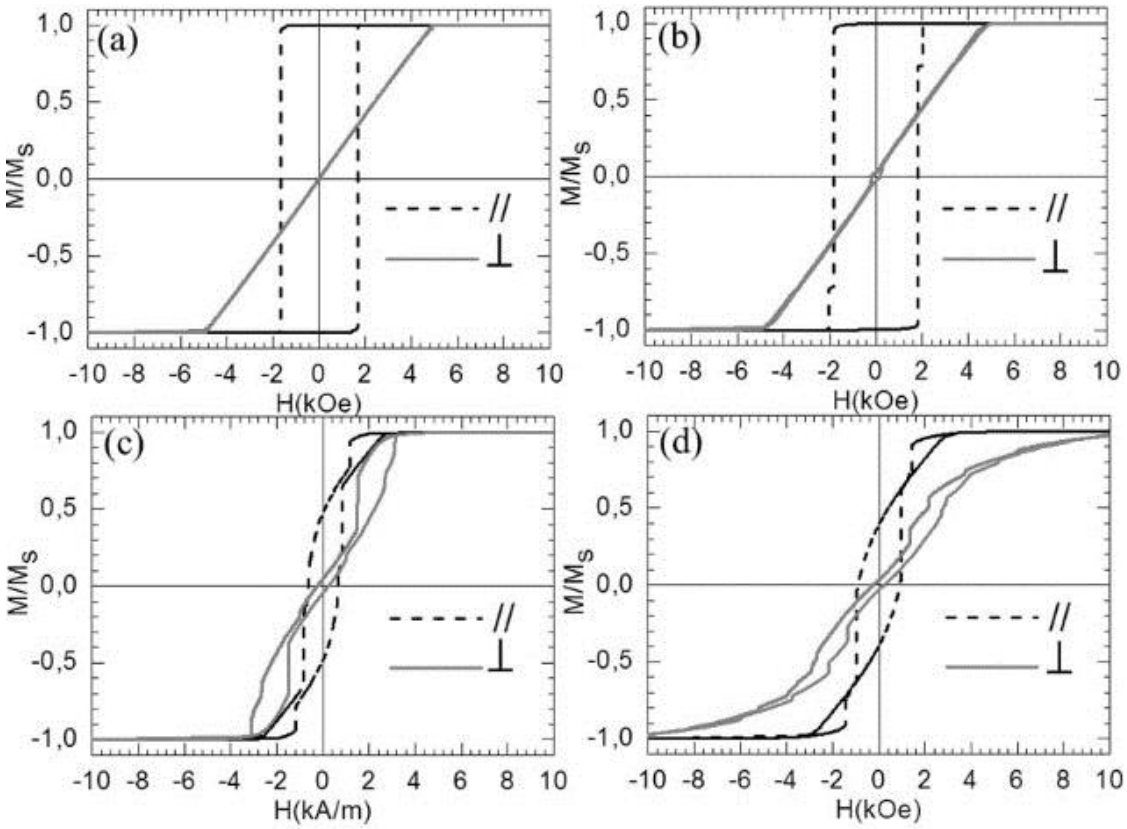

Figure 8. The typical hysteresis loops simulated for NWs which magnetic behavior is mostly determined by the shape anisotropy (a)-(b) and for NWs with strong competition of the shape and magnetocrystalline anisotropy(c)-(d). The simulations correspond to a single NW (a),(c) and hexagonal array of 7 NWs (b),(d) with 40 nm diameter and 105 nm inter-wire distances.

When the ratio diameter/interpore distance decreases, the magnetostatic interactions become more important. In general the experimental value of the coercivity of the arrays is less than the coercivity of the single NW (Vega, 2012). The experimental loop of the arrays of the NWs with dominated shape anisotropy is inclined [Nielsch, 2001; Paulus, 2001; Pan, 2005; Liu, 2008; Escrig, 2008; Vivas, 2012a; Salem, 2012] and does not show the one step magnetization reversal process as for single NW in the case of the magnetic field applied parallel to the NW axis. Such behavior is also reproduced in micromagnetic

simulations. Figure 9 shows the calculated magnetic loops for arrays of Co nanopillars with 75 nm diameter and 120 nm lengths. After taking into account the random distribution of the magnetocrystalline anisotropy direction and the increasing of the amount the nanopillars in the array (up to 49), the simulated loops fit very well the experimentally observed behavior (Vivas, 2013).

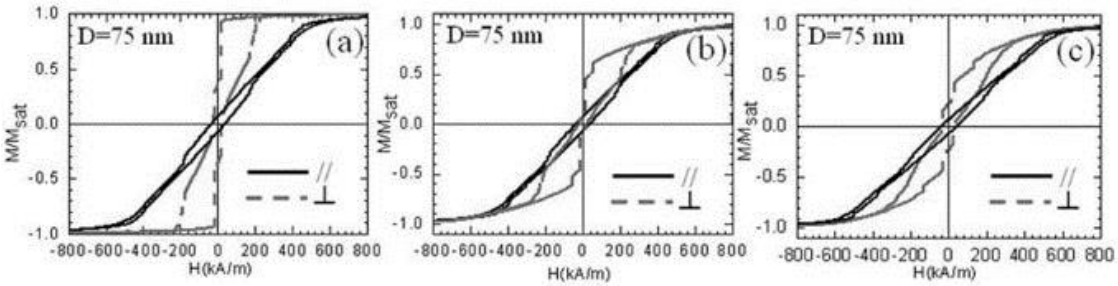

Figure. 9. The results of micromagnetic simulations of hysteresis loops of Co nanopillars arrays for D=75 nm: (a)- array of 7 nanopillars with the same magnetocrystalline easy axis for each nanopillar and the field applied parallel to it, (b) - array of 7 nanopillars with the random in-plane orientation of magnetocrystalline easy axes for each nanopillar, (c) - array of 19 nanopillars with random in-plane easy-axis distribution.

Another important effect is that in the simulations one should take into account the fact that different NWs are different by introducing defects promoting slightly different nucleation field. If NWs are modeled as granular with random easy distribution, this is automatically achieved. However, modeling of individual or small number of NWs can produce steps in hysteresis loops, not observed experimentally. The magnetostatic interactions normally smoothen the hysteresis curve, make the distribution of individual nucleation fields wider which changes significantly the coercivity and remanence of the array. By choosing the correct parameters and a sufficient number of simulated NWs, the

experimental magnetic behavior the NW's array can be successfully reproduced by micromagnetic simulation.

5. Future trends

Nowdays new technological perspectives are opened based on the control of magnetic states in magnetic nanoobjects by spin-polarised current rather than by magnetic field. In this direction, cylindrical magnetic nanowires attract significant interest due to their high potential in the development of novel memory devices constructed in 3D which can significantly increase the density of the memory. Additionally the magnetic based random access memory is expected to have much lower power consumption. Several micromagnetic studies have been performed to predict the most promising properties of the cylindrical NWs in terms of the aforementioned application.

Yan (2010) has shown by micromagnetic simulation that the current-induced motion of TDWs in cylindrical nanowires is fundamentally different from that in magnetic nanostripes. Domain wall velocity in nanostripes is limited due to the Walker breakdown phenomena. At some critical external magnetic field or electric current the periodical transformation of DW (TDW to VDW and vice versa) occurs and it slows the DW propagation. Micromagnetic simulations showed that the intrinsic pinning and the Walker limit do not exist for TDW in cylindrical NWs. It was attributed to a vanishing DW mass. The velocity of TDWs in a cylindrical nanowire simply depends linearly on the current density. Also the new method for the measurement of the nonadiabatic spin transfer torque parameter has been predicted based on the characteristics of the field- and the current-induced DW dynamics in cylindrical nanowires.

Later Wu (2014) proved the linear dependence of the DW velocity on the current density and the absence of the Walker breakdown in the case of the multiple current-induced TDWs motion (CIDWM) in cylindrical NWs by micromagnetic simulation. It has been shown that with an increase in the diameter the linear velocity of TDW decreases

correspondingly; but with the damping factor decreasing, the linear velocity increases. The results of micromagnetic simulations demonstrated that multiple CIDWM in cylindrical NWs provides an ideal way to control the DWs motion in magnetic nanodevices.

As we showed in the previous sections, there are two types of DWs in cylindrical NWs, depending on the NW diameter: For thinner NWs the TDW is favorable, for thicker – VDW (or Bloch point DW). Recently Piao (2013) studied micromagnetically the dynamics of the VDW in cylindrical NWs. The feature of this type of DW is the presence of a topological singularity in its center, a Bloch-point (BP) structure (Hertel, 2004). Actually, it is a complex three-dimensional (3D) spin structure, which is basically composed of two magnetic vortex structures with head-to head or tail-to-tail vortex cores. Recently topological singularities like skyrmions attracted a lot of interest due to promising application in data storage devices (Sampaio, 2013). In particular in Piao (2013) it has been found that there exists an intrinsic depinning field to trigger the VDW motion in cylindrical NWs. VDW propagates with a sequential single precessional switching of the BP core spin on a few picoseconds timescale, where a very fast VDW speed up to 2000 m/s is possible while keeping the structure of DW.

One of the promising issues on the way to realize the 3D memory device based on the cylindrical NWs is the creation of the periodic potential along the NW for DWs pinning. In Franchin (2011) the authors studied in details by micromagnetic simulations the effect of the pinning sites (with the size much less than the DW size) on the field- and current-driven DW motion in cylindrical NWs. In particularly they determined the critical fields and current densities required to push the DW through the barrier for various directions of the pinning potential. It has been found that the critical applied field decreases as the pinning direction gets orthogonal to the nanowire axis. Importantly, the critical current

density increases by more than a factor of 130 when the pinning direction gets orthogonal to the nanowire axis.

The ordered arrays of multilayered cylindrical nanowires is also very attractive for application in new generation of the microwave devices based on arrays of the spin-torque nanooscillators (Kiselev, 2003; Kaka, 2005; Dussaux, 2010). It has been shown by micromagnetic simulation of multilayered Co/Cu/Co nanowires (Abreu Araujo, 2012) that depending on the field amplitude and the injected dc current, a particular magnetic configurations appear, involving either a one-vortex state or a two-vortex magnetic state. The two-vortex states were found to be the most promising as microwave signals, originating from the GMR effect, and can be obtained without any static bias magnetic field. Recently it has been shown experimentally on the electrodeposited Co/Cu/Co nanowires embedded in AOT (Abreu Araujo, 2013).

Nowadays the new field in the magnetism, the so-called spin caloritronics, have received particular attention in the scientific community (Bauer, 2012). This is the combination of the thermoelectric effects with spintronics and nanomagnets. Thermal effects can be used to generate new functionalities in future spintronic devices. A challenge for device physics is to develop efficient devices for scavenging waste heat. Another issue is the imminent breakdown of Moore's law by the thermodynamic bottleneck: further decreases in feature size and transistor speed go in parallel with intolerable levels of ohmic energy dissipation associated with the motion of electrons in conducting circuits. Thermoelectric effects in nanostructures might help. Spin caloritronics studies the following phenomena: spin-dependent Seebeck/ Peltier coefficients and thermal conductance, thermal spin-transfer torques, spin and anomalous thermoelectric Hall effects, the recently discovered spin Seebeck effect and so on. Recently the first experimental measurements of the Seebeck coefficient in single cylindrical NW has been reported (Bohnert, 2013).

Micromagnetic studies are not trivial task in that case due to the thermal effects. Now most of them are focusing on the 2D nanostructures like Py nanostripes (Hinzke, 2011). However, the correct introduction of heating in micromagnetic simulations cannot be done based on the standard micromagnetic codes due to the assumption of a constant magnetization length. The micromagnetic approach based on the Landau-Lifshitz-Bloch (LLB) equation (Garanin, 1997; Chubykalo-Fesenko 2006) may be an option to overcome this limitation. Recently an extention of oommf micromagnetic code for the LLB equation has been created. It has been shown (Lebecki, 2012) that the LLB equation is more suitable for the Bloch point simulation than the standard micromagnetics. This opens a new possibility for modeling of DW propagation in cylindrical NWs moved by thermal gradients.

6. Further information

Main micromagnetic programs and their web pages.

Nowadays there are several micromagtetic packages available, both open source (Scholz, 2003; Donahue, 2006; Fischbacher, 2007) and commercial (Scheinfein, 2003; Berkov, 2007), allowing for reseachers to run their own simulations.

One of the frequently used public programs and tools for micromagnetics is the **OOMMF** (Object Oriented MicroMagnetic Framework) developed by the Applied and Computational Mathematics Division of the National Institute of Standards and Technology, USA. The code is being written in C++ with a Tcl/Tk. Program can be run in a wide range of Unix platforms and also Windows operation system. The open source scripting language Tcl/Tk is required to run OOMMF. The available free version is not parallel and solution is running only in one CPU. The parallel version is developing. Concerning the simulation of the cylindrical NWs, OOMMF allows to calculate a wide type of the problems such as: magnetic loops, DWs dynamics, multilayer structure, local fields etc. By using the special plugins it is possible to calculate the current-driven dynamics and in the nearest future the thermal effects. For cylindrical NWs the 3D solver and UNIX operation system must be used. OOMMF micromagnetics is based on the finite difference approachand the Fast Fourier transfor mfor magnetostatic field calculations. The model is completely symmetric and needs to take into account the effect of the edges due to the cubic mesh of the cylindrical NWs.

http://math.nist.gov/oommf/

In comparison, another free available micromagnetic tool is the **MAGPAR** (Parallel Finite Element Micromagnetics Package) developed by Werner Scholz. This software is an intrinsically parallel code and consequently can be run on several CPUs. Modern

working station with 12 CPU and 64 Gb RAM allows to perform, for example, the simulation of the NW's arrays (40-80 nm diameter, 1-2 μm length and 7-19 NWs in array) in quite reasonable period of time. Other advantage is the Finite element approximation. The model uses the finite elements tetrahedral mesh. There is no problem with the NW's shape, and intrinsic model symmetry, due to the distribution of the sizes of the elements it better reproduces the experimental results. Magpar package can be run only on the UNIX platforms. Also the special softwares for meshing and visualization are needed.

http://www.magpar.net/static/magpar/doc/html/index.html

Nmag [1] is a free open source micromagnetic simulation suite developed by Hans Fangohr's group at Southampton University (http://nmag.soton.ac.uk). Like Magpar, Nmag is based on a finite-element discretization of space and has the same advantages of more accurate description of non-cuboidal shapes over finite difference approaches, and the same disadvantages that mesh creation needs to be taken care of separately. Nmag is less tuned for performance than Magpar, and instead provides greater flexibility in its usage: an Nmag simulation script is a Python program that makes use of the Nmag library, and thus allows to carry out arbitrary scripted loops, decisions, use of saved data, postprocessing etc. Additional features include efficient data storage (binary compressed) in hdf5 files, and extraction into vtk files, support for arbitrary crystal anisotropy, periodic boundary conditions through the "macro geometry approach" in 1, 2 and 3 dimensions, and spin torque transfer terms, and postprocessing tools for magnonics. Nmag supports

[1] The authors thank Prof. J.Fangohr for writing this paragraph

use of the matrix compression library (HLib) for the boundary element matrix. One of Nmag's great strength is the extended documentation and tutorials available.

The one of the frequently used commercial software is the LLG **Micromagnetics Simulator™**, developed by Michael R. Scheinfein. This package has a very friendly graphical interface on Windows operation system. The last version is partially parallel. Very suitable for current driven dynamics, simulation of the spin-transport phenomena

and Ferromagnetic resonance measurements. The visualization part includes the possibility to simulate contrast produced by Magnetic force microscopy.

http://llgmicro.home.mindspring.com/AboutLLGFrame.htm

Another popular commercial micromagnetic software[2] is the package **MicroMagus**, developed and maintained over more than 15 years by Dmitry Berkov and Natalia Gorn. The package was initially intended for simulations of thin layer systems only, but later it was extended by the ability to study nanostructured elements of an arbitrary shape. The CPU-version of the software is parallelized and takes full advantage of the multicore processor architecture; very recently, the GPU-version has also been released. The standard package version for Windows contains a very intuitive and simple user-friendly interface, the version for Linux (without such an interface, but with the detailed instruction how to write the input files using any text editor) is available on demand. MicroMagus is a completely stand-alone tool, i.e. it does not require any additional software to run it or to vizualize the results (magnetization configurations obtained during simulations are saved into *bmp-files as color maps). The package employes a specially

[2] The authors thank Dr. D.Berkov for writing this paragraph

optimized energy minimization method for quasistatic simulations and advanced versions of the Runge-Kutta methods with the adaptive step-size control for dynamic simulations (including thermal fluctuations). MicroMagus is a finite-difference package. On the one side, this feature allows to use the great acceleration provided by FFT for the magnetodipolar field evaluation and simple high-accuracy approach for the computation of the exchange field. On the other side, this leads to standard difficulties in approximating the cylindrical form of the nanowires by the rectangular grid elements. However, in simulations with MicroMagus the approximation of shapes with curved borders can be substantially improved employing the rectangular elements with the 'partial' magnetization values assigned to those elements which cross the border of the ferromagnetic body under study.

Web site: http://www.micromagus.de

Finally, recently another software **GPMagnet** written specifically for the use on graphical processing units and CUDA has been created by the company GoParallel, based on Salamanca, Spain. The advantage is the possibility to increment substantially the calculation speed. This program also includes additional possibilities for spin-torque driven dynamics such Dzyaloshinskii-Moriya interactions and spin-orbit torques. The finite-difference discretization is used.

http://www.goparallel.net

7. References

Abreu Araujo, F., Darques, M., Zvezdin, K. A., Khvalkovskiy, A. V., Locatelli, N., Bouzehouane, K., Cros, V. and Piraux, L. (2012) 'Microwave signal emission in spin-torque vortex oscillators in metallic nanowires: Experimental measurements and micromagnetic numerical study', Phys. Rev. B, 86, 064424.

Abreu Araujo, F., Piraux, L., Antohe, V. A., Cros, V. and Gence, L. (2013) 'Phase locking of vortex-based spin-torque nanocontact oscillators by antivortices', Appl. Phys. Lett., 102, 222402.

Aharoni, A. (1997) 'Angular dependence of nucleation by curling in a prolate spheroid', J. Appl. Phys., 82, 1281.

Aharoni, A. (2000) Introduction to the Theory of Ferromagnetism, Oxford University Press.

Bauer, G. E. W., Saitoh, E. and van Wees, B. J. (2012) 'Spin caloritronics', Nature Mat., 11, 391.

Belliard, L., Miltat, J., Thiaville, A., Dubois, S., Duvail, J.L., Piraux, L. (1998) 'Observing magnetic nanowires by means of magnetic force microscopy', J. Magn. Magn. Mater., 190, 1–16.

Berkov, D.V. 'MicroMagus', http://www.micromagus.de/home.html.

Biziere, N., Gatel, C., Lassalle-Balier, R., Clochard, M. C., Wegrowe, J. E. and Snoeck, E. (2013) 'Imaging the Fine Structure of a Magnetic Domain Wall in a Ni Nanocylinder', Nano Lett., 13, 2053−2057.

Böhnert, T., Vega, V., Michel, A.-K., Prida, V. M., Nielsch, K. (2013) 'Magneto-thermopower and magnetoresistance of single Co-Ni alloy nanowires', Appl. Phys. Lett., 103, 092407.

Boulle, O., Malinowski, G., Klaui, M. (2011) 'Current-induced domain wall motion in nanoscale ferromagnetic elements', Materials Science and Engineering R, 72, 159–187.

Bran, C., Ivanov, Yu. P., Garcia, J., del Real, R. P., Prida, V. M., Chubykalo-Fesenko, O. and Vazquez, M. (2013) 'Tuning the magnetization reversal process of FeCoCu nanowire arrays by thermal annealing', J. Appl. Phys., 114, 043908.

Bran, C., Ivanov, Yu. P., Trabada, D. G., Tomkowicz, J., del Real, R. P., Chubykalo-Fesenko, O. and Vazquez, M. (2013) 'Structural Dependence of Magnetic Properties in Co-Based Nanowires: Experiments and Micromagnetic Simulations', IEEE Trans. Magn., 49, 4491.

Brown, W. F. (1963) 'Thermal Fluctuations of a Single-Domain Particle', Phys. Rev., 130, 1677.

Brown, W. F. (1963) Micromagnetics, New York, Wiley.

Chang, M.-T., Chou, L.-J., Hsieh, C.-H., Chueh, Y.-L., Wang, Z. L., Murakami, Y. and Shindo D. (2007) 'Magnetic and Electrical Characterizations of Half-Metallic Fe3O4 Nanowires', Adv. Mater., 19, 2290–2294.

Choi, D. S., Hopkins, X., Kringel, R., Park, J., Jeon, I. T. and Kim, Y. K. (2012) 'Magnetically driven spinning nanowires as effective materials for eradicating living cells', J. Appl. Phys., 111, 07B329.

Choi, D.S., Park, J., Kim, S., Gracias, D.H., Cho, M.K., Kim, Y.K., Fung, A., Lee, S.E., Chen, Y., Khanal, S., Baral, S. and Kim, J.H. (2008) 'Hyperthermia with Magnetic Nanowires for Inactivating Living Cells', J. Nanosci. Nanotechnol., 8, 2323-2327.

Cullity, B. D. (1972) Introduction to Magnetic Materials, Reading, MA: Addison-Wesley.

Chubykalo-Fesenko, O., Nowak, U., Chantrell, R.W. and Granin (2006), D."Dynamics approach for micromagnetic close to the Curie temperature", Phys. Rev. B, 74, 094436

Da Col, S., Jamet, S., Rougemaille, N., Locatelli, A., Mentes, O. T., Santos Burgos, B., Afid, R., Darques, M., Cagnon, L., Toussaint, J. C. and Fruchart, O. (2014) 'Observation of Bloch-point domain walls in cylindrical magnetic nanowires', Phys. Rev. B, 89, 180405(R).

Donahue, M. and Porter, D. (2006) 'Object Oriented Micromagnetic Framework (OOMMF)', The National Institute of Standards and Technology (NIST), http://math.nist.gov/oommf/

Dussaux, A., Georges, B., Grollier, J., Cros, V., Khvalkovskiy, A.V., Fukushima, A., Konoto, M., Kubota, H., Yakushiji, K., Yuasa, S., Zvezdin, K.A., Ando, K. and Fert, A. (2010) 'Large microwave generation from current-driven magnetic vortex oscillators in magnetic tunnel junctions', Nat. Commun., 1, 8.

Escrig, J., Altbir, D., Jaafar, M., Navas, D., Asenjo, A. and Vazquez, M. (2007) 'Remanence of Ni nanowire arrays: Influence of size and labyrinth magnetic structure', Phys. Rev. B, 75, 184429.

Escrig, J., Lavin, R., Palma, J. L., Denardin, J. C., Altbir, D., Cortes, A. and Gomez, H. (2008) 'Geometry dependence of coercivity in Ni nanowire arrays', Nanotechnology, 19, 075713.

Fernandez-Pacheco, A., Serrano-Ramon, L., Michalik, J. M., Ibarra, M. R., De Teresa. J. M., O'Brien. L., Petit, D., Lee, J. and Cowburn, R. P. (2013) 'Three dimensional magnetic nanowires grown by focused electron-beam induced deposition', Scientific Reports, 3, 1492.

Fert, A. and Piraux, L. (1999) 'Magnetic nanowires', J. Magn. Magn. Mater., 200, 338.

Fischbacher, T., Franchin, M., Bordignon, G. and Fangohr, H. A (2007) 'Systematic Approach to Multiphysics Extensions of Finite-Element-Based Micromagnetic Simulations: Nmag', IEEE Transactions on Magnetics, 43, 2896-2898.

Fisher, J. E. (1970) 'Structure and magnetic anisotropy of f.c.c. cobalt films between 150° and 870 °K', Thin Solid Films, 5, 53.

Forster, H., Schrefl, T., Dittrich, R., Suess, D., Scholz, W., Tsiantos, V., Fidler, J., Nielsch, K., Hofmeister, H., Kronmuller, H., Fischer, S. (2002) 'Magnetization reversal in granular nanowires', IEEE Trans. Magn., 38, 2580.

Franchin, M., Knittel, A., Albert, M., Chernyshenko, D. S., Fischbacher, T., Prabhakar, A. and Fangohr, H. (2011) 'Enhanced spin transfer torque effect for transverse domain walls in cylindrical nanowires', Phys. Rev. B, 84, 094409.

Fung, A. O., Kapadia, V., Pierstorff, E., Ho, D. and Chen, Y. (2008) 'Induction of Cell Death by Magnetic Actuation of Nickel Nanowires Internalized by Fibroblasts', J. Phys. Chem. C, 112, 15085-15088.

Garanin, D. A. (1997) 'Fokker-Planck and Landau-Lifshitz-Bloch equations for classical ferromagnets', Phys. Rev. B, 55, 3050.

Haehnel, V., Fahler, S., Schaaf, P., Miglierini, M., Mickel, C., Schultz, L. and Schlorb, H. (2010) 'Towards smooth and pure iron nanowires grown by electrodeposition in self-organized alumina membranes', Acta Mater., 58, 2330.

Henry, Y., Ounadjela, K., Piraux, L., Dubois, S., George, J.-M. and Duvail, J.-L. (2001) 'Magnetic anisotropy and domain patterns in electrodeposited cobalt nanowires', Eur. Phys. J. B, 20, 35.

Hertel, R. (2002) 'Computational micromagnetism of magnetization processes in nickel nanowires', J. Magn. Magn. Mater. 249, 251.

Hertel, R. and Kirschner, J. (2004) 'Magnetization reversal dynamics in nickel nanowires', Physica B, 343, 206.

Hinzke, D., Nowak, U. (2011) 'Domain Wall Motion by the Magnonic Spin Seebeck Effect', Phys. Rev. Lett., 107, 027205.

Ivanov, Yu. P., Vazquez, M. and Chubykalo-Fesenko, O. (2013) 'Magnetic reversal modes in cylindrical nanowires', J. Phys. D: Appl. Phys., 46, 485001.

Ivanov, Yu. P., Vivas, L. G., Asenjo, A., Chuvilin, A., Chubykalo-Fesenko, O. and Vazquez, M. (2013) 'Magnetic structure of a single-crystal hcp electrodeposited cobalt nanowire', Europhys. Lett., 102, 17009.

Kaka, S., Pufall, M. R., Rippard, W. H., Silva, T. J., Russek, S. E. and Katine, J. A. (2005) 'Mutual phase-locking of microwave spin torque nano-oscillators', Nature 437, 389- 392.

Kim, K., Xu, X., Guo, J. and Fan D. L., (2014) 'Ultrahigh-speed rotating nanoelectromechanical system devices assembled from nanoscale building blocks', Nature Commun., 5, 3632.

Kiselev, S. I., Sankey, J. C., Krivorotov, I. N., Emley, N. C., Schoelkopf, R. J., Buhrman, R. A. and Ralph, D. C. (2003) 'Microwave oscillations of a nanomagnet driven by a spin-polarized current', Nature, 425, 380-383.

Lavín, R., Denardin, J. C., Escrig, J., Altbir, D., Cortés, A. and Gómez, H. (2009) 'Angular dependence of magnetic properties in Ni nanowire arrays', J. Appl. Phys., 106, 103903.

Lebecki, K. M. and Donahue, M. J. (2010) 'Comment on "Frustrated magnetization in Co nanowires: Competition between crystal anisotropy and demagnetization energy", Phys. Rev. B, 82, 096401.

Lebecki, K. M., Hinzke, D., Chubykalo-Fesenko, O. and Nowak U. (2012) 'Key role of temperature in ferromagnetic Bloch point simulations', Phys. Rev. B, 86, 094409.

Lee, B. Y., Heo, K., Schmucker, A. L., Jin, H. J., Lim, J. K., Kim, T., Lee, H., Jeon, K.-S., Suh, Y. D., Mirkin, C. A. and Hong, S. (2012) 'Nanotube-Bridged Wires with Sub-10 nm Gaps', Nano Lett., 12, 1879−1884.

Lee, J., Suess, D., Schrefl, T., Oh, K. H. and Fidler, J. (2007) 'Magnetic characteristics of ferromagnetic nanotube', J. Magn. Magn. Mater., 310, 2445.

Liao, Z.-M., Li, Y.-D., Xu, J., Zhang, J.-M., Xia, K. and Yu, D.-P. (2006) 'Spin-Filter Effect in Magnetite Nanowire', Nano Lett., 6, 1087-1091.

Liu, Y., Sellmyer, D. J. and Shindo, D. (2005) Handbook of Advanced Magnetic Materials: Nanostructural Effects, v. 1, Berlin. Springer.

Liu, Z., Chang, P.-C., Chang, C.-C., Galaktionov, E., Bergmann, G. and Lu, J. G. (2008) 'Shape Anisotropy and Magnetization Modulation in Hexagonal Cobalt Nanowires', Adv. Funct. Mater., 18, 1573.

Mayergoyz, D. J. (1985) 'Hysteresis models from the mathematical and control theory points of view', J. Appl. Phys. 57, 3803.

Navas, D., Asenjo, A., Jaafar, M., Pirota, K. R., Hernandez-Velez, M., Sanz, R., Lee, W., Nielsch, K., Batallan, F. and Vazquez, M. (2005) 'Magnetic behavior of NixFe(100−x) (65⩽x⩽100) nanowire arrays', J. Magn. Magn. Mater., 290–291, 191.

Nielsch, K., Wehrspohn, R. B., Barthel, J., Kirschner, J., Gosele, U., Fischer, S. F. and Kronmuller, H. (2001) 'Hexagonally ordered 100 nm period nickel nanowire arrays', Appl. Phys. Lett., 79, 1360.

Nielsch, K.,Wehrspohn, R. B., Barthel, J., Kirschner, J., Fischer, S. F., Kronmuller, H., Schweinbock, T., Weiss, D. and Gosele, U. (2002) 'High density hexagonal nickel nanowire array', J. Magn. Magn. Mater., 249, 234.

Nikulina, E., Idigoras, O., Vavassori, P., Chuvilin, A. Berger, A. (2012) 'Magneto-optical magnetometry of individual 30 nm cobalt nanowires grown by electron beam induced deposition', Appl. Phys. Lett., 100, 142401.

Pan, H., Liu, B., Poh, J. Yi, Ch,, Lim, S., Ding, J., Feng, Y., Huan, C. H. A. and Lin, J. (2005) 'Growth of Single-Crystalline Ni and Co Nanowires via Electrochemical Deposition and Their Magnetic Properties', J. Phys. Chem. B, 109, 3094.

Parkin, S. S. P., Hayashi, M. and Thomas, L. (2008) 'Magnetic Domain-Wall Racetrack Memory', Science, 320, 190-194.

Paulus, P. M., Luis, F., Kroll, M., Schmid, G. and de Jongh, L. J. (2001) 'Low-temperature study of the magnetization reversal and magnetic anisotropy of Fe, Ni, and Co nanowires', J. Magn. Magn. Mater., 224, 180.

Piao, H.-G., Shim, J.-H., Djuhana, D. and Kim, D.-H. (2013) 'Intrinsic pinning behavior and propagation onset of three-dimensional Bloch-point domain wall in a cylindrical ferromagnetic nanowire', Appl. Phys. Lett., 102, 112405.

Reddy, S. M., Park, J. J., Na, S.-M., Maqableh, M. M., Flatau, A. B. and Stadler, B. J. H. (2011) 'Electrochemical Synthesis of Magnetostrictive Fe–Ga/Cu Multilayered Nanowire Arrays with Tailored Magnetic Response', Adv. Funct. Mater., 21, 4677–4683.

Rheem, Y., Yoo, B.-Y., Beyermann, W. P. and Myung, N.V. (2007) 'Magnetotransport studies of a single nickel nanowire', Nanotechnology, 18, 015202.

Rheem, Y., Yoo, B.-Y., Koo, B. K., Beyermann, W. P. and Myung, N. V. (2007) 'Synthesis and magnetotransport studies of single nickel-rich NiFe nanowire', J. Phys. D: Appl. Phys., 40, 7267–7272.

Safi, M., Yan, M., Guedeau-Boudeville, M.-A., Conjeaud, H., Garnier-Thibaud, V., Boggetto, N., Baeza-Squiban, A., Niedergang, F., Averbeck, D., Berret, J.-F. (2011) 'Interactions between Magnetic Nanowires and Living Cells: Uptake, Toxicity, and Degradation', ACS Nano, 5, 5354–5364.

Salem, M. S., Sergelius, P., Zierold, R., Montero Moreno, J. M., Gorlitz, D. and Nielsch, K. (2012) 'Magnetic characterization of nickel-rich NiFe nanowires grown by pulsed electrodeposition', J. Mater. Chem., 22, 8549.

Sampaio, J., Cros, V., Rohart, S., Thiaville, A. and Fert, A. (2013) 'Nucleation, stability and current-induced motion of isolated magnetic skyrmions in nanostructures', Nature Nanotech., 8, 839.

Scheinfein, M., R. 'LLG Micromagnetics SimulatorTM', http://llgmicro.home.mindspring.com/index.htm.

Scholz, W., Fidler, J., Schrefl, T., Suess, D., Dittrich, R., Forster, H. and Tsiantos, V. (2003) 'Scalable parallel micromagnetic solvers for magnetic nanostructures', Comput. Mater. Sci., 28, 366.

Schroeder, P., Schotter, J., Shoshi, A., Eggeling, M., Bethge, O., Hutten, A. and Bruckl, H. (2011) 'Artificial cilia of magnetically tagged polymer nanowires for biomimetic mechanosensing', Bioinsp. Biomim. 6, 046007.

Sekhar, M. C., Liew, H. F., Purnama, I., Lew, W. S., Tran, M., and Han, G. C. (2012) 'Helical domain walls in constricted cylindrical NiFe nanowires', Appl. Phys. Lett., 101, 152406.

Sellmyer, J., Zheng, M. and Skomski, R. (2001) 'Magnetism of Fe, Co and Ni nanowires in self-assembled arrays', J. Phys: Condens. Matter., 13, R433.

Serrano-Ramón, L., Córdoba, R., Rodríguez, L. A., Magén, C., Snoeck, E., Gatel, C., Serrano, I., Ibarra, M. R. and De Teresa, J. M. (2011) 'Ultrasmall Functional Ferromagnetic Nanostructures Grown by Focused Electron-Beam-Induced Deposition', ACS Nano, 5, 7781-7787.

Smith, N., Markham, D., LaTourette, D. (1989) 'Magnetoresistive measurement of the exchange constant in varied-thickness permalloy films', Journ. Appl. Phys., 65, 4362.

Song, M.-M., Song, W.-J., Bi, H., Wang, J., Wu, W.-L., Sun, J., Yu, Min. (2010) 'Cytotoxicity and cellular uptake of iron nanowires', Biomaterials, 31, 1509.

Spinu, L., Stancu, A., Radu, C., Li, F., Wiley, J.B. (2004) 'Method for magnetic characterization of nanowire structures', IEEE Transactions on Magnetics, 40, 2116-2118.

Stancu, A., Pike, C., Stoleriu, L., Postolache, P., Cimpoesu, D. (2003) 'Micromagnetic and Preisach analysis of the First Order Reversal Curves (FORC) diagram', J. Appl. Phys., 93, 6620-6622.

Stoleriu, L., Pinzaru, C. and Stancu, A. (2012) 'Micromagnetic analysis of switching and domain structure in amorphous metallic nanowires', Appl. Phys. Lett., 100, 122404.

Thiaville, A., Garcia, J.M., Dittrich, R., Miltat, J. amd Schrefl, T. (2003) "Micromagnetic study of Bloch points nucleated vortex core reversal" Phys. Rev. B., 67, 094410

Usov, N. A., Antonov, A.S., Lagar'kov, A.N. (1998) 'Theory of giant magneto-impedance effect in amorphous wires with different types of magnetic anisotropy', J. Magn. Magn. Mater., 185, 159-173.

Usov, N. A., Peschany, S.E. (1993) 'Magnetization curling in a fine cylindrical particle', J. Magn. Magn. Mater., 118, L290-L294.

Vazquez, M. and Vivas, L. G. (2011) 'Magnetization reversal in Co-base nanowire arrays', Phys. Status Solidi b, 248, 2368.

Vega, V., Bohnert, T., Martens, S., Waleczek, M., Montero-Moreno, J. M., Gorlitz, D., Prida, V. M. and Nielsch, K. (2012) 'Tuning the magnetic anisotropy of Co-Ni nanowires:

comparison between single nanowires and nanowire arrays in hard-anodic aluminum oxide membranes', Nanotechnology, 23, 465709.

Vila, L., Darques, M., Encinas, A., Ebels, U., George, J.-M., Faini, G., Thiaville, A. and Piraux, L. (2009) 'Magnetic vortices in nanowires with transverse easy axis', Phys. Rev. B, 79, 172410.

Vivas, L. G., Escrig, J., Trabada, D. G., Badini-Confalonieri, G. A. and Vazquez, M. (2012) 'Magnetic anisotropy in ordered textured Co nanowires', Appl. Phys. Lett., 100, 252405.

Vivas, L. G., Ivanov, Yu. P., Trabada, D. G., Proenca, M. P., Chubykalo-Fesenko, O. and Vazquez, M. (2013) 'Magnetic properties of Co nanopillar arrays prepared from alumina templates', Nanotechnology, 24, 105703.

Vivas, L. G., Vazquez, M., Escrig, J., Allende, S., Altbir, D., Leitao, D. C. and Araujo, J. P. (2012) 'Magnetic anisotropy in CoNi nanowire arrays: Analytical calculations and experiments', Phys. Rev. B, 85, 035439.

Vivas, L. G., Yanes, R., Chubykalo-Fesenko, O. and Vazquez, M. (2011) 'Coercivity of ordered arrays of magnetic Co nanowires with controlled variable lengths', Appl. Phys. Lett., 98, 232507.

Wang, J. B., Zhou, X. Z., Liu, Q. F., Xue, D. S., Li, F. S., Li, B., Kunkel, H. P. and Williams, G. (2004) 'Magnetic texture in iron nanowire arrays', Nanotechnology, 15, 485.

Wu, F.-S., Horng, L. and Wu, J.-C. (2014) 'Fast Moving Multiple Magnetic Bits in Permalloy Cylindrical Nanowires', IEEE Transactions on Magnetics, 50, 1401004.

Yan, M., Kákay, A., Gliga, S. and Hertel, R. (2010) 'Beating the Walker Limit with Massless Domain Walls in Cylindrical Nanowires', Phys. Rev. Lett., 104, 057201.

Yang, S. G., Zhu, H., Yu, D. L., Jin, Z. Q., Tang, S. L. and Du, Y. W. (2000) 'Preparation and magnetic property of Fe nanowire array', J. Magn. Magn. Mater., 222, 97.

Zhang, J., Jones, G.A., Shen, T. H., Donnelly, S. E. and Li, G. H. (2007) 'Monocrystalline hexagonal-close-packed and polycrystalline face-centered-cubic Co nanowire arrays fabricated by pulse dc electrodeposition', J. Appl. Phys., 101, 054310.

Zheng, M., Menon, L., Zeng, H., Liu, Y., Bandyopadhyay, S., Kirby, R. D. and Sellmyer, D. J. (2000) 'Magnetic properties of Ni nanowires in self-assembled arrays', Phys. Rev. B, 62, 12282.